Particle-In-Cell simulation of electrostatic waves in the ionosphere

Rakesh Moulick[1], Sayan Adhikari[2,3], Gunjan Sharma[1], Wojciech J. Miloch[3], and B. K. Saikia[1]

[1]Centre of Plasma Physics, Institute for Plasma Research
[2]Institute for Energy Technology
[3]Department of Physics, University of Oslo

March 27, 2023

Abstract

In the space atmosphere, plasma with two electron components is very common. The cold species of electron ($T_e \sim 1$ eV) usually originate in the ionosphere, while the hot electron species ($T_e \sim 100$ eV) appear from the magnetosphere. In addition to these two electron species, there may be a beam of electrons streaming along the magnetic field lines. These electrons are responsible for exciting various electrostatic wave modes. Several authors have investigated such a system in the recent past. In this article, we revisit the problem and provide some more beam energy-based systemic insights.

Particle-In-Cell simulation of electrostatic waves in the ionosphere

R. Moulick[1], S. Adhikari[2,3], G. Sharma[1], B. K. Saikia[1] and W. J. Miloch[2]

[1]Centre of Plasma Physics, Institute for Plasma Research, Nazirakhat, Sonapur-782402, Kamrup(M), Assam, India

[2]Department of Physics, University of Oslo, PO Box 1048 Blindern, NO-0316 Oslo, Norway

[3]Institute for Energy Technology, Instituttveien 8, 2007 Kjeller, Norway

Key Points:

- 1D-1V electrostatic Particle-In-Cell simulation has been used to investigate the evolution of electrostatic waves in an unmagnetized plasma.
- There are three species of electrons in the system, with one streaming with a finite drift velocity replicating the ionospheric conditions.
- The streaming electrons are believed to be responsible for exciting various electrostatic wave modes in the plasma.

Corresponding author: S. Adhikari, `sayan.adhikari@ife.no`

Abstract

In the space atmosphere, plasma with two electron components is very common. The cold species of electron ($T_e \sim 1$ eV) usually originate in the ionosphere, while the hot electron species ($T_e \sim 100$ eV) appear from the magnetosphere. In addition to these two electron species, there may be a beam of electrons streaming along the magnetic field lines. These electrons are responsible for exciting various electrostatic wave modes. Several authors have investigated such a system in the recent past. In this article, we revisit the problem and provide some more beam energy-based systemic insights.

Plain Language Summary

This paper deals with the electron dynamics and instabilities occurring in the ionosphere. There are three electron components, namely the cold, hot, and beam electrons, with static background ions. It has been observed that the three-species electron interaction gives rise to non-linear behavior in terms of sharing of kinetic energies among the species. The hot electrons are more responsive to the initial beam energy and drain the lion's share of it. However, there are instances when the beam also gets back its share from the hot and the cold species. Broadband Electrostatic Noise (BEN) as observed in the space atmosphere, is often associated with the presence of multi species of electrons. Such phenomena are of critical importance for the exploration of the space. Thus, The results will certainly be beneficial for deeper understanding of the ionospheric phenomena.

1 Introduction

The Sun's magnetic activity oscillates periodically ($\sim$ 11 years) leading to solar activities such as solar flares and coronal mass ejections (Karak et al., 2018). The coronal mass brings with it a stream of highly energetic particles which travels roughly at a speed of 270 km/sec. The Earth's magnetosphere is responsible for restricting majority of these particles from entering into the Earth's neutral atmosphere. Besides, the solar ultraviolet radiation ionizes a portion of the Earth's neutral atmosphere, and due to infrequent collisions resulting in slow recombination, a permanent ionized atmosphere is formed, which is known as the ionosphere. The Earth has its ionosphere beginning at around 60 km from the surface and extending up into the magnetosphere, which starts from around 500 km above the Earth's surface (Cowley, 2007). The ionosphere act like a sink for many highly energetic particles coming from the Sun. Therefore, most of the matter in the ionosphere is in the ionized state, in the form of plasma. However, binary collisions, which are common in most of the laboratory plasmas, are rare in ionospheric plasmas. Hence, such plasma is collisionless to a greater extent(Parks, 2019). Ionosphere is the home to many satellites including the GPS satellites. Being the first layer for the satellite signals, change in the ionospheric conditions have deep influence on the electromagnetic waves used for navigation and communications (Sharifi & Farzaneh, 2016; Langley, 2000).

The study of the plasma environments in space, particularly those of the Earth, Mars, and the Jovian atmospheres, has gained wide popularity in recent times(Garrett et al., 2016; Russell, 2010). The knowledge of the electrodynamics phenomena happening in the Earth's atmosphere exemplifies similar dynamics in other planetary systems as well. The Earth's ionosphere is further responsible for the Broadband Electrostatic Noise (BEN), that are high and low frequency electrostatic fluctuations (S. Singh et al., 2009). The magnetic field aligned electron beams act as the free energy sources in the polar cusp region of the Earth. These beam electrons along with a coexisting source of hot and cold electrons may explain the Broadband Electrostatic Noise (Lu et al., 2005; S. Singh et al., 2009; Lin et al., 1984; Tokar & Gary, 1984). Therefore, this paper has the motivation to demonstrate and discuss the electrostatic wave phenomena happening in the Earth's upper atmosphere.

There are many papers that discuss the phase space and bipolar electric field structures appearing in the ionosphere especially on the basis of the FAST satellite observations (Goldman et al., 2000; Crary et al., 2001; Newman et al., 2001). The bipolar electric field structures are associated with the two stream instabilities and appear when the instability saturates. The non-linear evolution of such instabilities give rise to the phase space holes.

Our concern in this paper is the interaction among the electron population of three different types, namely the hot, cold, and beam electrons available in the ionosphere. The cold species originate in the ionosphere, while the hot electrons often appear from the magnetosphere. Besides, a stream of energetic electrons, low in density, may appear following the magnetic field lines and disturb the coexisting system of the hot and cold electrons. Such beams act like free energy sources triggering streaming instabilities in the plasma, which was brought to light by Bohm and Gross (1949). The appearance of bipolar field structures and phase space holes in such a system has been observed by Lu et al. (2005). We investigate the phase space for similar appearance along with the mode of energy transfer in the light of Particle-In-Cell simulation.

A good insight into the physics of beam-plasma interactions could be manifested largely via particle simulations. Kinetic studies enable us to explore the enriching physics of beam-plasma systems that are relevant to the ionospheric environment. For example, Dum (1990) had shown, for a relatively colder beam, primarily, the beam mode is excited with a growth rate slightly below the plasma frequency. A transition from reactive to kinetic instability is caused by the broadening of the beam, where the drift energy of the beam is gradually lost to the electric field. This, in turn, excites wave modes of larger wave numbers. Since various oscillatory modes can be present in a beam-plasma system, the wave-wave interaction processes also have a vital role to play. A forward propagating beam-excited Langmuir wave can merge with an existing ion acoustic mode and consequently generate a backward propagating ion-acoustic wave (Kasaba et al., 2001). This process is responsible for the transfer of energy from one Langmuir wave to another via wave-wave coupling and is thought to be the initial step of type III radio emission (Ginzburg & Zheleznyakov, 1958). In a Vlasov-Poisson simulation of the solar wind, Henri et al. (2010) have shown that the electrostatic decay of beam-driven Langmuir waves is possible when ion temperature is close to the electron temperature. Such energy transfer processes from one mode/species to another are key to many physical observations. In this regard, an important finding has been reported by An et al. (2017). In a PIC simulation study, they have shown that in the presence of a magnetic field, for a gyrating field-aligned electron beam, the energy transfer rate is faster between the electron beam and electrostatic waves, resulting in the suppression of the whistler instability by the electrostatic instability. Furthermore, Chakrabarti and Sengupta (2009) have highlighted the nonlinear interaction of the electron acoustic and electron plasma waves. Keeping in mind the possibilities of these dynamic phenomena, the concern in the present paper has been kept to understand the mode of energy transfer among the particles and analyze their phase space during the interaction.

In the following, section II deals with the simulation model, section III deals with the results, and finally, the paper has been concluded in section IV.

2 Simulation Model

There are three components of electrons in the model. Ions being massive and non-responsive to the fast oscillating electric fields of electrons, are considered to form a neutral background. The total unperturbed electron density is $n_{e0} = n_{c0}+n_{h0}+n_{b0}$ where, n_{c0}, n_{h0} and n_{b0} denote the unperturbed density of the cold, hot and beam electrons respectively. The plasma frequency of the j^{th} species is written as

$$\omega_{pj} = \left(\frac{n_{j0}e^2}{m_e\epsilon_0}\right)^{\frac{1}{2}} \tag{1}$$

The Debye length of the j^{th} species is given by:

$$\lambda_{Dj} = \left(\frac{\epsilon_0 T_j}{n_{j0}e^2}\right)^{\frac{1}{2}} \tag{2}$$

The analytical expressions for the dispersion relations corresponding to the electron acoustic wave, electron plasma wave, and electron beam wave, respectively are given by (Koen et al., 2012)

$$\omega^2 = \omega_{pc}^2\left(\frac{1+3k^2\lambda_{Dc}^2}{1+1/k^2\lambda_{Dh}^2}\right) \tag{3}$$

$$\omega^2 = \omega_{pc}^2\left(1+3k^2\lambda_{Dc}^2\right) + \omega_{ph}^2\left(1+3k^2\lambda_{Dh}^2\right) \tag{4}$$

$$\omega = \frac{ku_d}{1+n_b/n_{e0}} \approx ku_d \tag{5}$$

The Particle-In-Cell code "SPIC (PIC for Space Plasmas)[1]" has been developed to study the system under consideration. SPIC is a one-dimensional electrostatic code with periodic boundary conditions. The creation of one's own code is thought to offer more implementation control and flexibility. The code can be expanded to implement any further requirement. The code considers the electrons and ions as raw simulation particles, and initial velocity distribution has been sampled out of a Maxwellian distribution for all the species. However, the beam electrons have a streaming speed, in addition to their Maxwellian component. The system under consideration is collisionless with no ambient magnetic field. The code has been fully normalized with the following normalization scheme.

$t' = w_p t$, where ω_p is the total electron plasma frequency and 't' is time

[1] https://github.com/rakeshmoulick/SPIC

$x' = x/\lambda_D$ where, λ_D is the characteristic Debye length corresponding to the temperature of the cold electrons (T_{ec}) and the total equilibrium density n_0. Thus,

$$\lambda_D = \left(\frac{\epsilon_0 T_{ec}}{n_0 e^2}\right)^{\frac{1}{2}} \tag{6}$$

$v' = v/v_{Tc} = v/(\omega_{pc}\lambda_{Dc})$ where, v_{Tc} is the thermal velocity of the cold electron species.

$\phi' = e\phi/T_{ec}$ where, T_{ec} is the cold electron temperature and

$E' = \left(\frac{e}{m_e \omega_p^2 \lambda_D}\right) E$

The governing equations of the system (to be simulated via Particle-In-Cell), thus, become:

$$\frac{d^2\phi'}{dx'^2} = -\left(N_i - N_{ec} - N_{eh} - N_{eb}\right) \tag{7}$$

$$E' = -\left(\frac{T_{ec}}{m_e \omega_p^2 \lambda_D^2}\right)\frac{d\phi'}{dx'} \tag{8}$$

$$v' = \left(\frac{q}{m}\right)\left(\frac{T_{ec}}{e}\right)\left(\frac{1}{\omega_p \omega_{pc} \lambda_D \lambda_{Dc}}\right) E' t' \tag{9}$$

$$x = \left(\frac{\omega_{pc}}{\omega_p}\right)\left(\frac{\lambda_{Dc}}{\lambda_D}\right) v' t' \tag{10}$$

2.1 Simulation Setup

We consider a one-dimensional simulation domain that has been divided into 1024 cells, the size of each cell being equal to λ_D. The cell spacing in the normalized unit stands for unity. The time step has been considered as $0.01\omega_{pe}^{-1}$. All densities have been normalized by the cold electron density and velocities are expressed in the units of the thermal velocity of the cold electrons. There are 5 million pseudo-particles launched for each species of electrons. The code has been written using the parsing utility "ini-parser", which splits the input variables into an "input.ini" file. Python scripts (can be found in the aforementioned GitHub repository) were used to post-process the data.

2.2 Discretization and Charge Density Calculation

The one-dimensional Poisson's equation is discretized as follows (Changmai & Bora, 2019; Birdsall & Langdon, 2004; Brieda, 2019):

$$\frac{\phi_{i-1} - 2\phi_i + \phi_{i+1}}{\Delta x^2} = \frac{\rho_i}{\epsilon_0}$$

The subscript "i" denote the value of the concerned physical quantity at the middle of the cell. Consequently, the electric field is given as follows:

$$E_i = -\frac{\phi_{i+1} - \phi_i}{\Delta x}$$

The charge density at the grid location is calculated from the particle position using the standard method of scattering.

$$\rho = \sum_{j=1}^{N} = q_j n_j$$

Where, q_j and n_j are the charge and number density of the species "j".

The Poisson's solver which solves for the plasma potential in the domain has been implemented via direct and Gauss-Seidel methods. However, for fast execution, use of a direct solver is suggested.

3 Results and Discussion

We investigate several distinct cases as shown in Table 1. The results are depicted for a wide range of beam speed. Additionally, Run-8 has the hot electron population increased by 10 times than the cold electrons. Other parameters are relevant to the upper ionospheric region. It is possible to see that the ionospheric parameters change, depending on the solar activity by comparing the IRI (*International Reference Ionosphere*, n.d.) and Solar Progression Cycle (*Space Weather Prediction Center SOLAR CYCLE PROGRESSION*, n.d.) data. For example, Fig 1 shows the electron density and temperature profiles on the 1^{st} February 2014 and 2020 at 77.8750°N, 20.9752°E (Svalbard). This chosen coordinate is reasonably at high latitude and the Earth's magnetic field lines are parallel to the particle flow direction. The observed deviation of the parameters in Fig 1 is primarily due to the Sun's activity, which is higher in 2014 than it is in 2020. Usually, there are two distinct populations of electrons in the ionosphere (Marif & Lilensten, 2020). The first ones are the ambient thermal electrons, whose temperature is on the order of electron volts or even less than that. The second is the population of high energetic electrons having temperature on the order of several kilo electron volts. The high energetic electrons originate due to two main reasons. First, due to the photo-ionization by Extreme Ultra Violet (EUV) radiation, and second, due to Energetic Electron Precipitation (EEP). Originally, the precipitated electrons appear from the solar wind and solar flares. It is important to note that the solar flare electrons are potentially highly energetic, typically, $10-20$ million K in temperature, which, may become as high as 100 million K (Holman & Benedict, n.d.). Furthermore, during geomagnetic storms, the magnetosphere and the ionosphere can become strongly coupled and in such a case, the precipitating electrons can reflect back to the magnetosphere. This, in turn, influences the total precipitating flux in the upper ionosphere (about 800 km) (Khazanov et al., 2019).

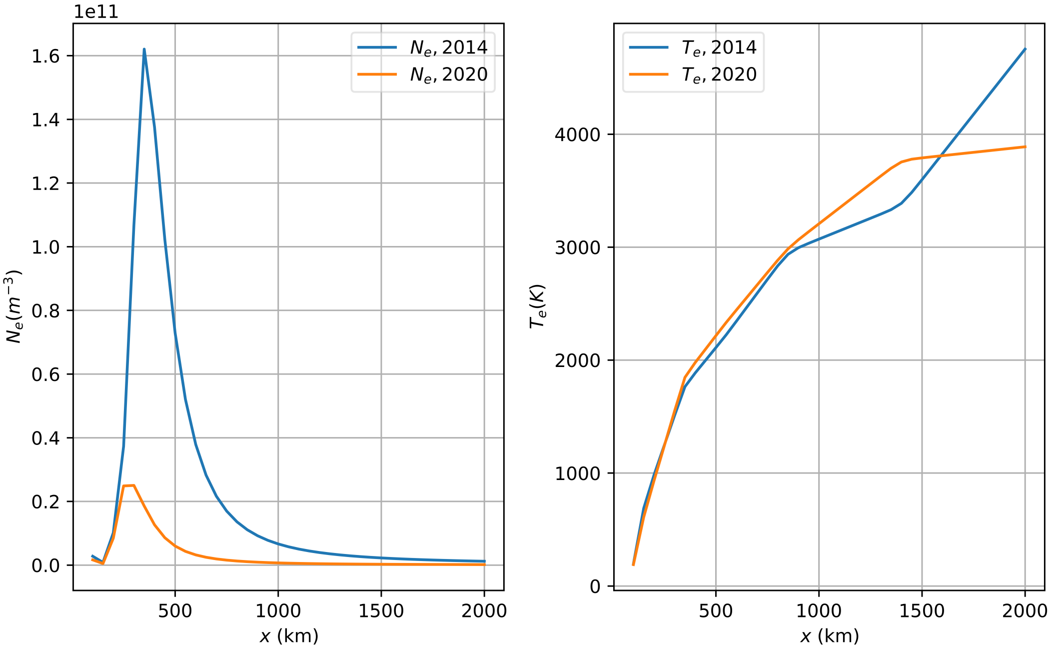

Figure 1: Plot of the electron density and temperature profiles on 1st Feb 2014 and 2020 at Svalbard (77.8750°N, 20.9752°E).

In this article, the cold electron temperature has been maintained at $1eV$ ($\sim 11600K$) (Slight variation with the actual data should not disturb the physical aspect of our point of interest). More details on the ionospheric electron temperature are available at (Dalgarno et al., 1963). We maintain the hot electron temperature at $100eV$ ($\sim 1160452.5K$). In addition, the system contains beam electrons, which enter the system by following the magnetic field lines. We assume the system to be in a state, such that, the hot and the cold electrons are not in thermal equilibrium with each other.

Table 1: Simulation parameters for various runs.

Run	$\alpha = n_{h0}/n_{c0}$	$\beta = n_{b0}/n_{c0}$	$\theta = T_h/T_c$	$\phi = T_h/T_b$	$\upsilon_d = u_d/\upsilon_{Tc}$
1	1.0	0.04	100.0	100.0	15
2	1.0	0.04	100.0	100.0	20
3	1.0	0.04	100.0	100.0	25
4	1.0	0.04	100.0	100.0	35
5	1.0	0.04	100.0	100.0	40
6	1.0	0.04	100.0	100.0	45
7	1.0	0.04	100.0	100.0	80
8	10.0	0.04	100.0	100.0	40

Fig 2 shows the plot of the kinetic energy at various time instances for a low beam energy ($\upsilon_d = 20$, where, $\upsilon_d = u_d/\upsilon_{Tc}$). The plot shows the drainage of kinetic energy from the beam to the hot and cold electron species respectively. While the kinetic energies of the hot and the cold species increase, a steadiness is set approximately beyond $\omega_{pe}t = 250$. Fig 3 shows the corresponding dispersion graph of the system. There are three modes that are supposed to be excited in the presence of a beam (Lu et al., 2005; Koen et al., 2012). Out of these, the Langmuir mode or the electron plasma wave is seen to be excited along with the electron acoustic mode. The modes are well-matched with the analytical curves. However, the beam mode represented by the solid line is almost indistinguishable in the dispersion plot.

Fig 4 shows the kinetic energy plot of the three electronic systems at relatively high beam energy ($\upsilon_d = 80$). It is interesting to observe that although there is a dissipation of the beam energy to the hot and cold electron species, the beam again receives back a portion of energy from the hot and the cold species. Thus, in two consecutive instances, there is a bi-directional exchange of energy occurring between the beam and the other

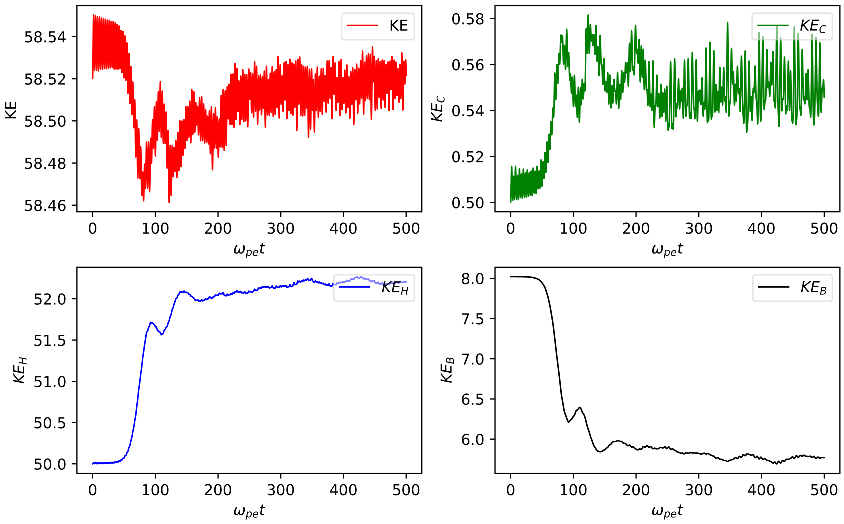

Figure 2: Plot of the kinetic energy (in normalized units) for $v_d = 20$.

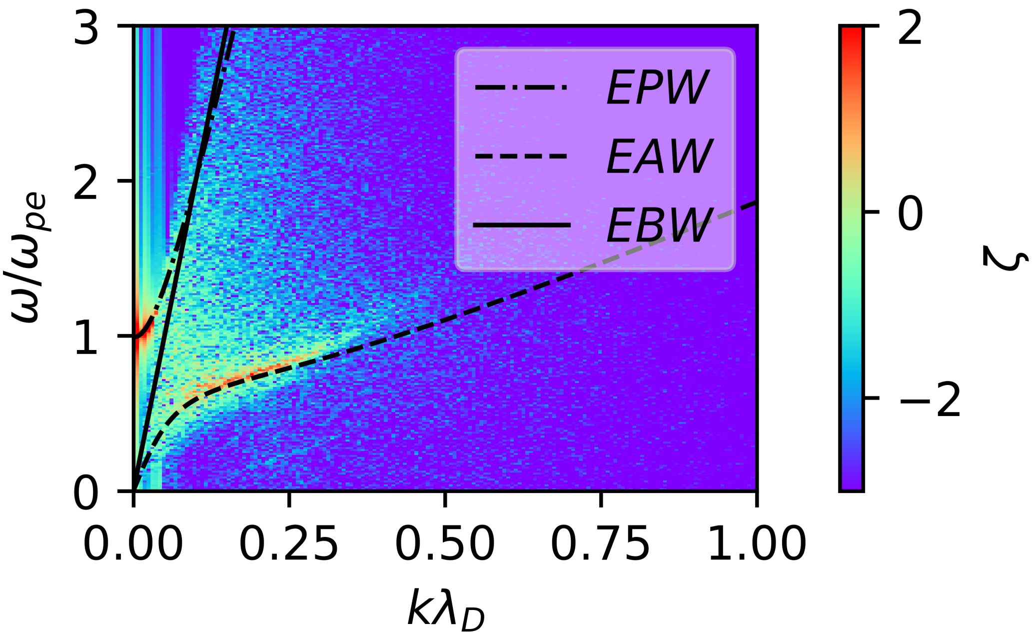

Figure 3: Dispersion relation of the resulting system for $v_d = 20$. ζ represents the FFT amplitude of the normalized electric field.

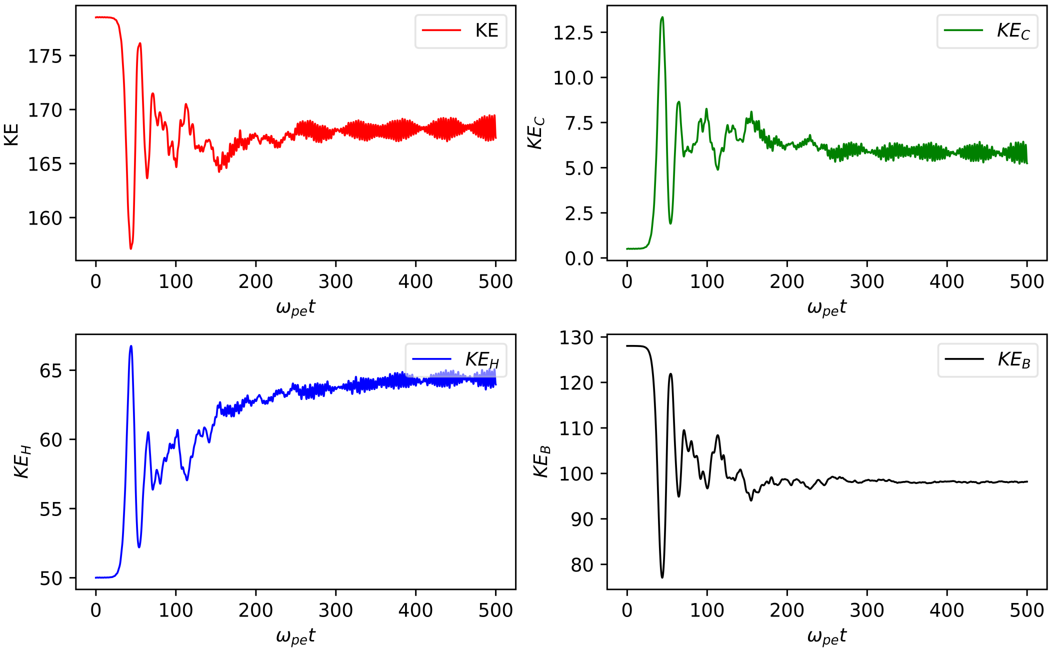

Figure 4: Plot of the kinetic energy (in normalized units) for $v_d = 80$.

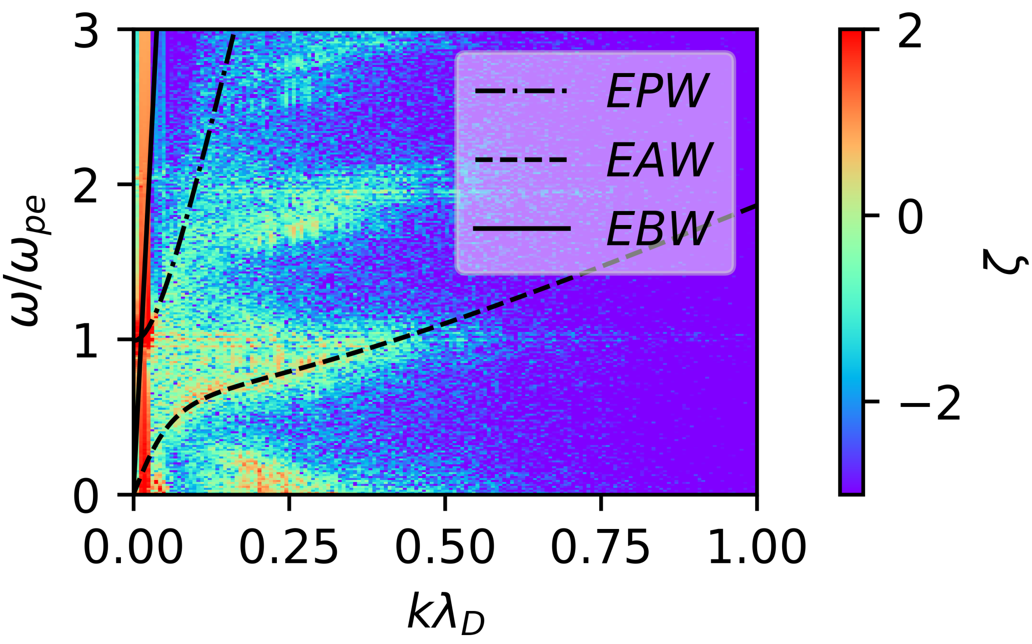

Figure 5: Dispersion relation of the resulting system for $v_d = 80$. ζ represents the FFT amplitude of the normalized electric field.

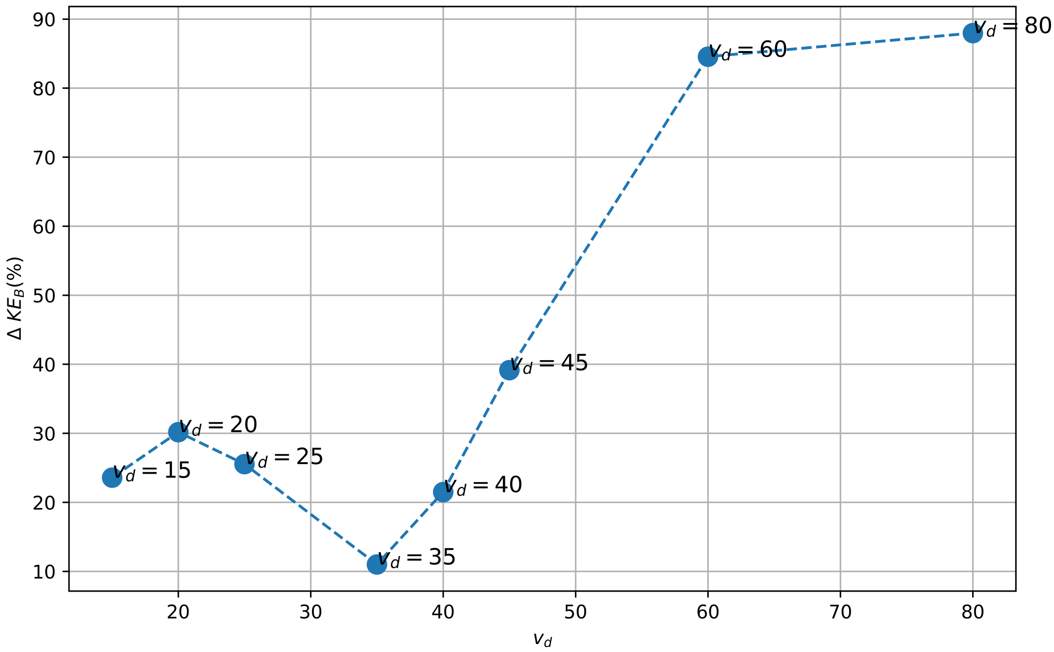

Figure 6: Percentage of the beam kinetic energy retrieval at different values of υ_d.

two species. The dispersion plot of the resulting system is shown in Fig 5. At such high beam energy, the beam mode is prominent unlike the case of low beam energy. Alongside this, the Langmuir mode and the electron acoustic modes are also observed. An important point to notice here is that the electron acoustic mode is more damped as compared to the previous case. In general, if the beam streaming speed is below the thermal speed of the hot electrons, the beam mode vanishes. However, above this limiting speed of the beam, the electron acoustic mode is amplified with a reduction in the beam energy (Gary & Tokar, 1985; Lu et al., 2005). In Fig 5, the beam energy is more, and hence, the electron acoustic mode is damped. The dispersion plot also captures the higher harmonics of the electron plasma wave and the electron acoustic wave.

At this point, it is important that we investigate the percentage retrieval of the beam kinetic energy and show the variation with υ_d. By percentage retrieval we mean, the amount of energy retrieved by the beam from the background electrons at the instant of highest recovery (e.g. for $\upsilon_d = 80$, $\omega_{pe}t = 50$ approximately). Fig 6 shows the overall percentage of the beam kinetic energy retrieval ($\Delta KE_B(\%)$) at different values of the parameter υ_d. We observe an interesting trend with a sharp rise in the energy retrieval from

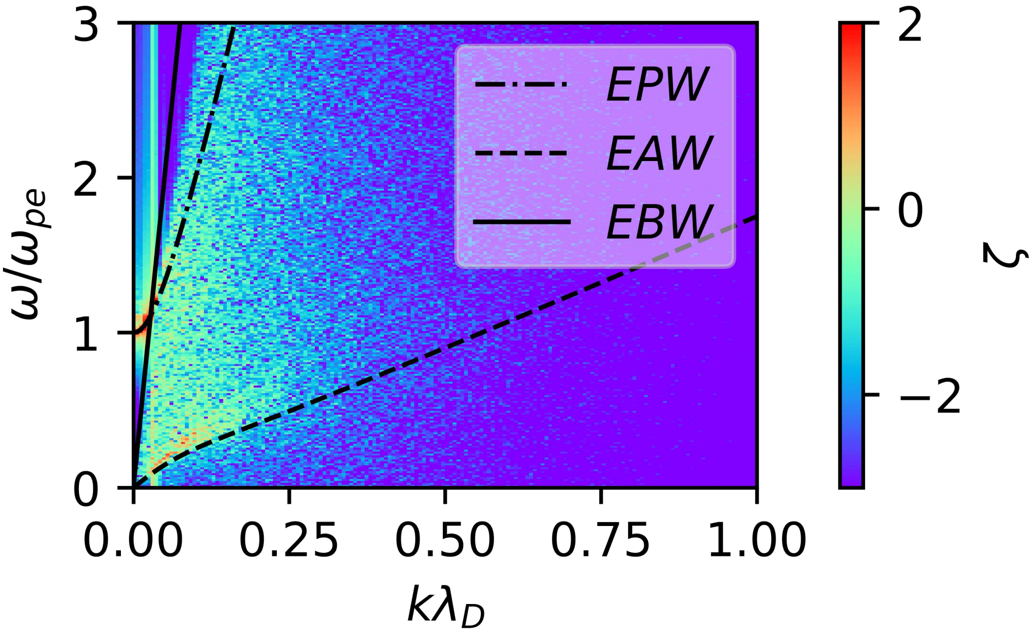

Figure 7: Dispersion relation corresponding to Run-8. ζ represents the FFT amplitude of the normalized electric field.

$v_d = 35$ to $v_d = 60$. Overall, the energy retrieval process seems to be non-linear with respect to the initial beam energy.

Fig 7 and Fig 8 shows the dispersion graph and the kinetic energy profiles of the three electron system respectively for $\alpha = 10$ (Run-8). In this case, the hot electron population is 10 times greater than the cold electron population. We observe a good comparison of the numerical and analytical expressions in the dispersion relation. We further investigate into the sum total of potential and kinetic energy of the system. Fig 9 shows the total energy evolution of the system at $v_d = 20$. We observe, the potential and kinetic energy evolve opposite of each other, thereby keeping a constant total energy. This in turn, shows the conservation of energy in the system. For all other higher values of the parameter v_d, we observe a constant total energy. The electrostatic potential energy has been calculated using $U = \frac{\epsilon_0}{2}\int_v E^2 dv$, where, dv is a small element of volume. Fig 10 and fig 11 shows the contribution of the cold and hot electrons on the electron acoustic wave for $v_d = 20$. While the acoustic character due to the cold group of electrons is prominent at moderately high value of the wave number, the hot electrons are responsible for the same at low wave number. Fig 12 and fig 13 shows the phase

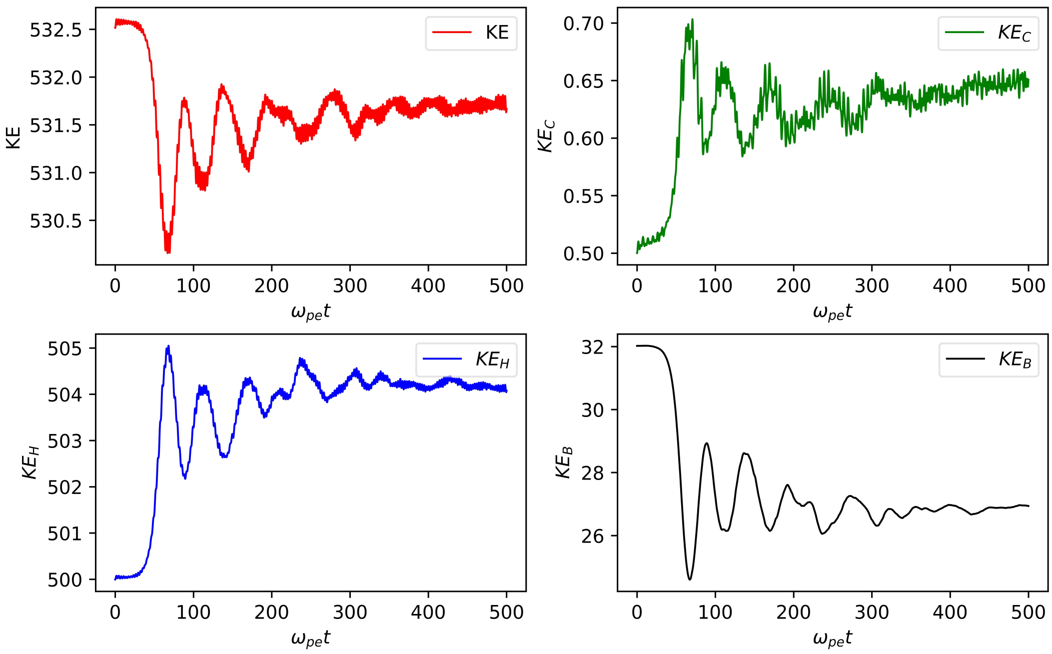

Figure 8: Plot of the Kinetic Energy (in normalized unit) for Run-8.

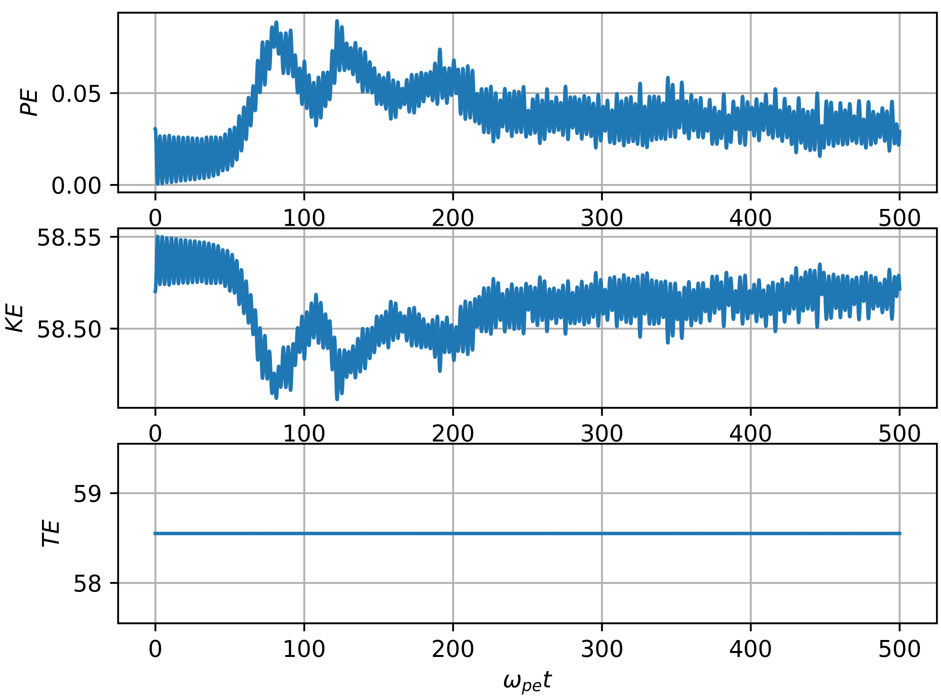

Figure 9: Plot of the total Energy (in normalized unit) for $v_d = 20$. Here, PE stands for the potential energy, KE for kinetic energy and TE implies the total energy of the system.

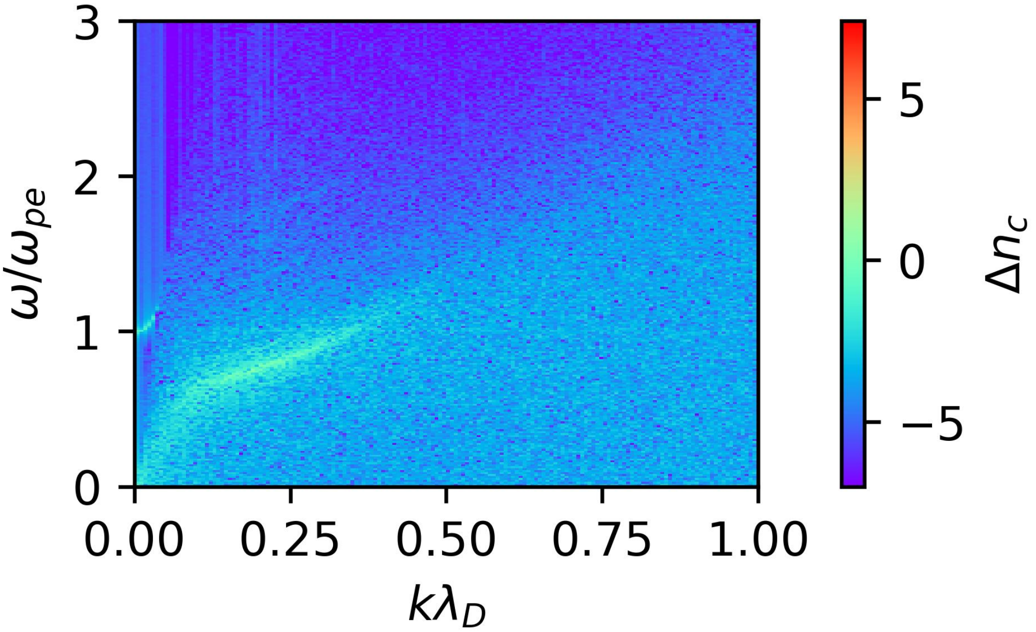

Figure 10: Density fluctuation FFT (Δn_c) of the cold electrons at $v_d = 20$.

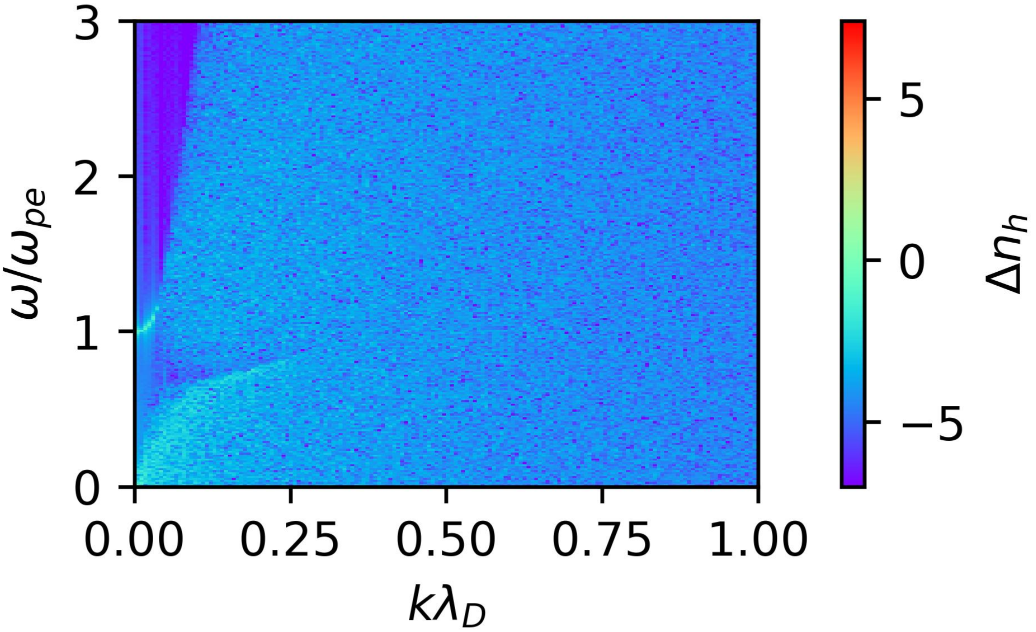

Figure 11: Density fluctuation FFT (Δn_h) of the hot electrons at $v_d = 20$.

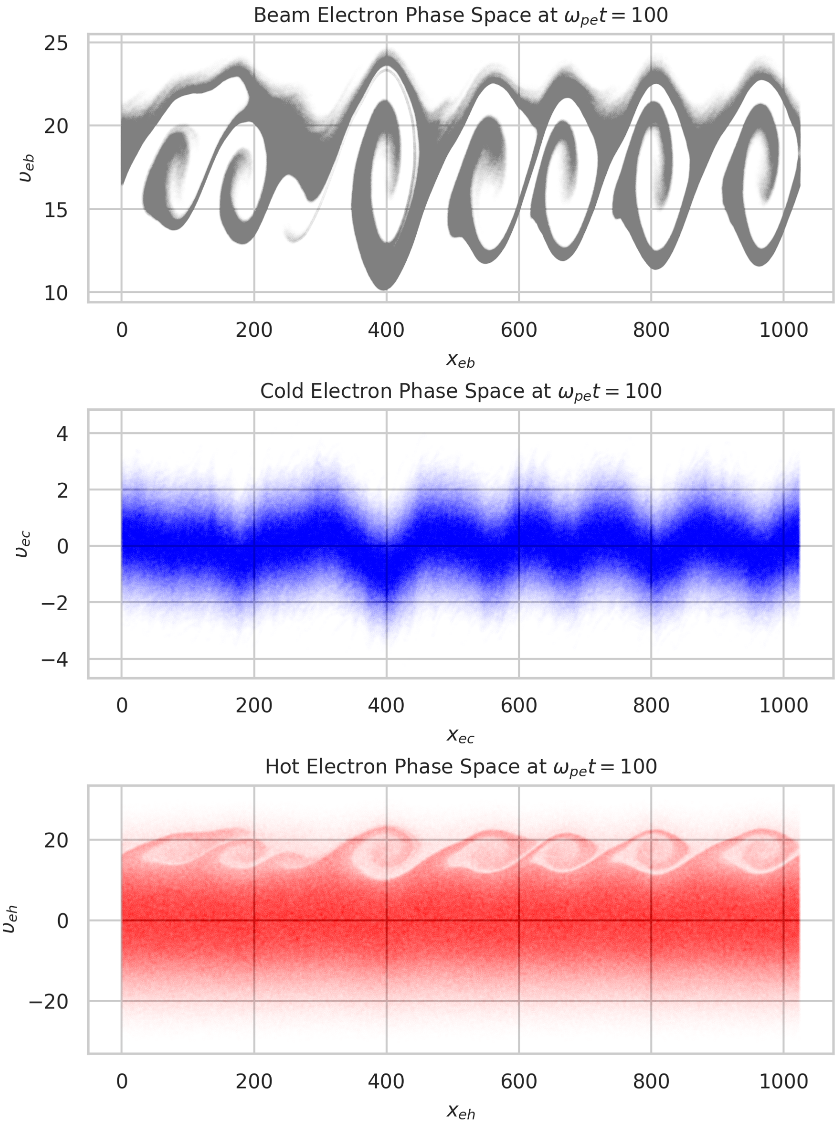

Figure 12: Phase space plot at $\upsilon_d = 20$ for $\omega_{pe}t = 100$.

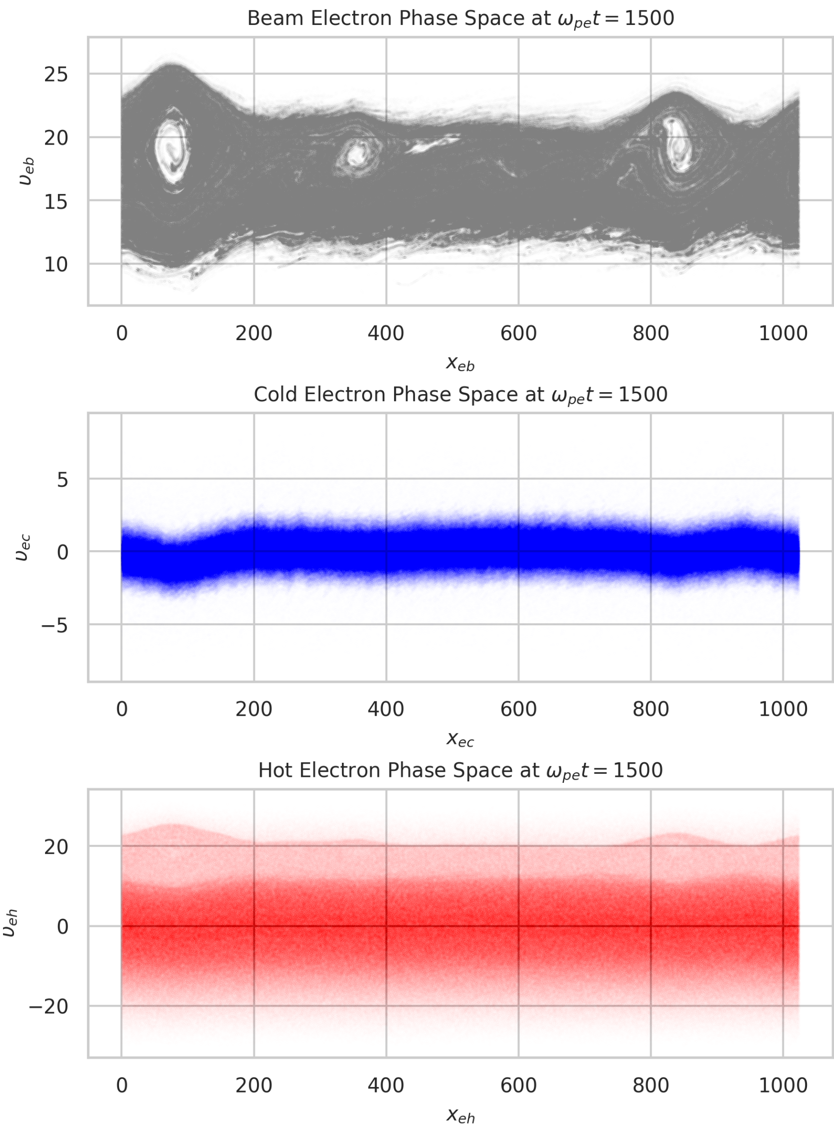

Figure 13: Phase space plot at $\upsilon_d = 20$ for $\omega_{pe}t = 1500$.

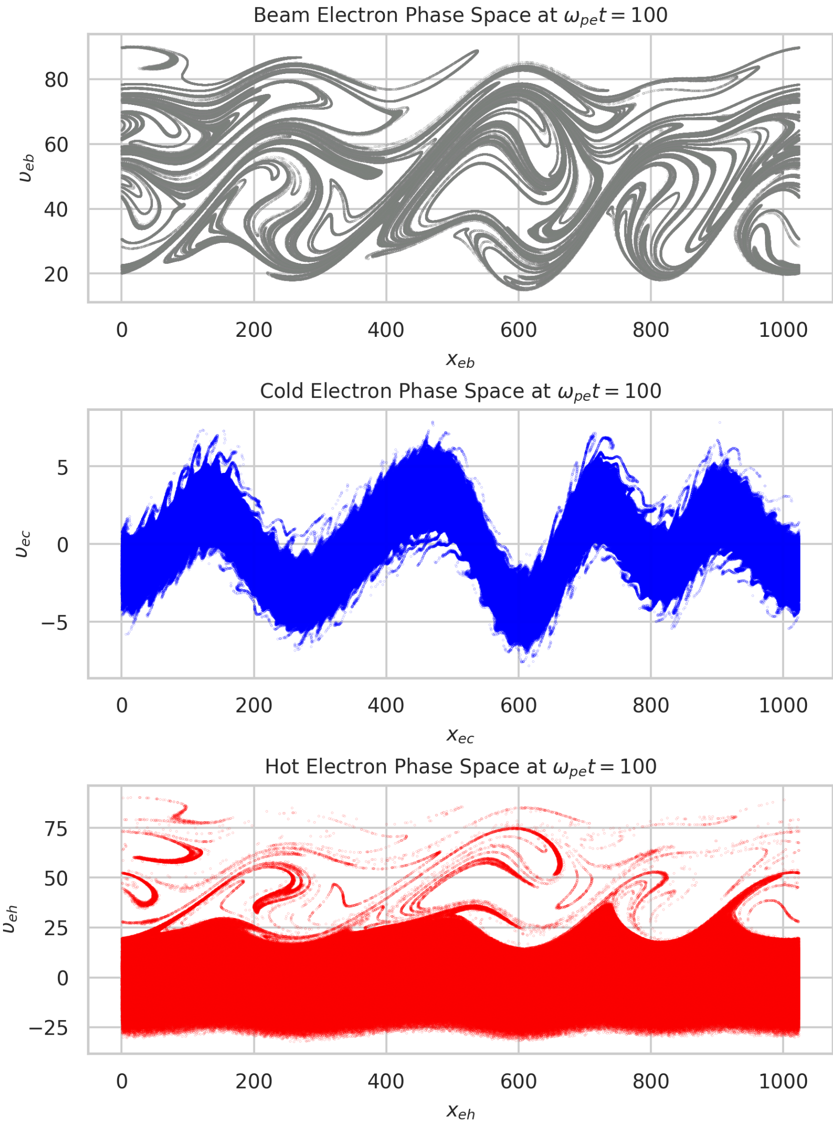

Figure 14: Phase space plot at $\upsilon_d = 60$ for $\omega_{pe}t = 100$.

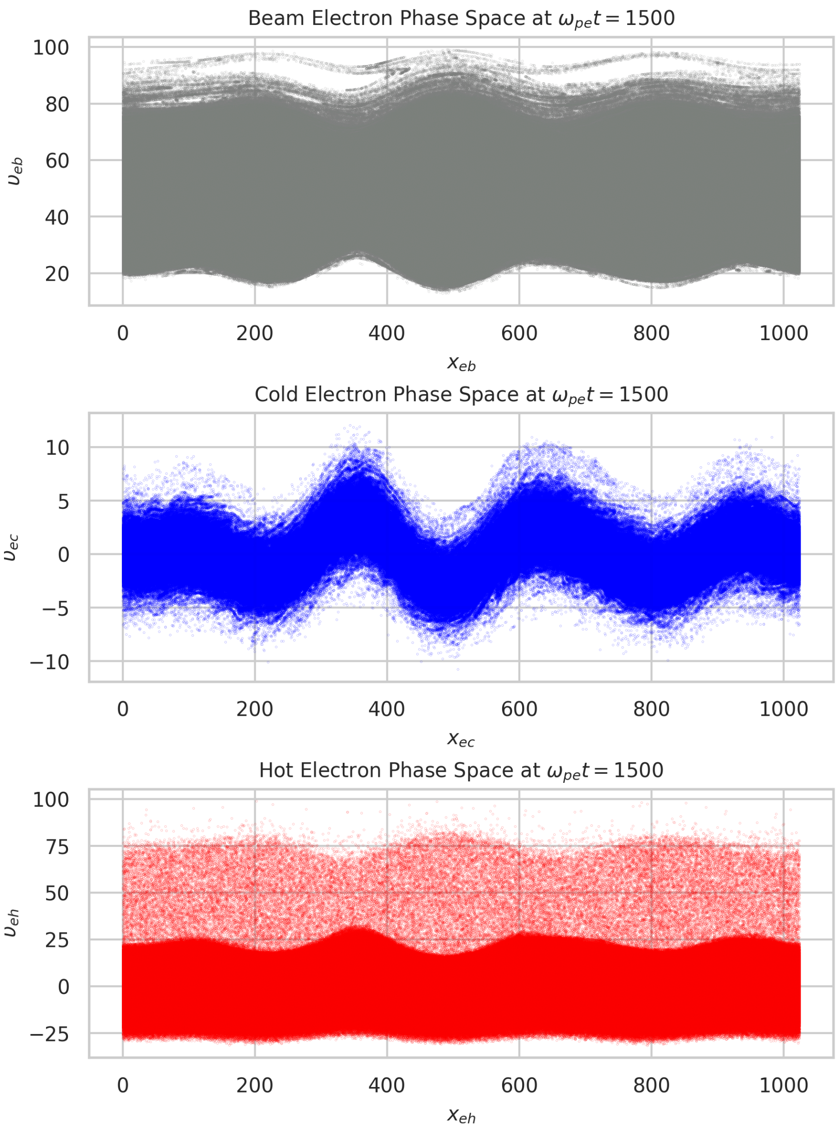

Figure 15: Phase space plot at $v_d = 60$ for $\omega_{pe}t = 1500$.

space plot of the beam, cold and hot electrons at two different instances ($\omega_{pe}t = 100$ and $\omega_{pe}t = 1500$) respectively for $\upsilon_d = 20$. While the first one shows the onset of instability, the second one is saturated. It can easily be observed (12) that the hot electron vortices have smaller spread in velocity, however, approximately the same spatial size as the beam electrons . The beam has an overall positive velocity distribution. We consider the positive x-direction to be the motion of the beam. As the beam progresses, the hot electrons traveling in the same direction are highly disturbed. The magnitude of the disturbance on the cold electrons is relatively weak; however, it happens in a bi-directional way. Therefore, very weak vortex formation is observed for both positive and negative velocities. Once the instabilities are saturated, many vortices are merged together in the beam, and we observe two major holes in the phase space (13). Similar structures were also observed in the simulation results of Lu et al. (2005). These are often known as the Bernstein-Green-Kruskal (BGK) electron holes. Experimentally, these correspond to the solitary potential structures, which move at a speed much greater than the ion acoustic speed. An analysis of such phase space holes have been presented in Muschietti et al. (1999). The fact that electron beams are responsible for the generation of electrostatic solitary waves has been reported in (Omura et al., 1996), via a one-dimensional PIC simulation of two electron beams and an ion beam traveling along the static magnetic field. More such simulations in two and three dimensions are available in the literature (Jao & Hau, 2016; Miyake et al., 1998, 2000; N. Singh et al., 2000). Fig 14 and fig 15 on the other hand shows the phase space at those two instances for higher beam velocity $\upsilon_d = 60$. With higher beam speed, hot electrons are seen to form stronger vortices, while, the disturbance in the cold electrons become prominent. In addition, the vortex size of the beam is also enhanced. The correlation between the spatial sizes of the hot and beam electron vortices is in fact intriguing to examine.

4 Conclusion

The paper aims at understanding electron dynamics and its effects on the Earth's ionosphere. The region is rich in non-linear dynamic phenomena. Mutual interactions of the hot and cold electrons in the presence of a beam has portrayed several interesting facts. The following are some of the critical observations:

1. It has been observed that the kinetic energy plays an important role. Usually, there is a dominant energy transfer from the beam to the other species of electrons, how-

ever, at high beam energies, a portion of the energy is instantaneously regained by the beam from the other electron species. This retrieval is non-linearly related to the initial beam energy, although, we see a sharp and almost linear transition from $v_d = 35$ to $v_d = 60$.

2. The cold electrons are observed to be affected bidirectionally by the presence of the beam, while the hot electron has a unidirectional effect. Furthermore, the hot electrons respond more to the presence of the beam and are heavily disturbed. The spatial vortex sizes of the beam and hot electrons are highly correlated.
3. Although both cold and hot electrons participate towards the acoustic behaviour of the electrons, the cold electrons contribute at moderate wave number (k), whereas, the hot electrons contribute at lower values of the wave number.

Acknowledgments

The simulations for the work described in this paper were performed on **ANTYA**, an HPC Linux Cluster, IPR, Gujarat, India.

References

An, X., Bortnik, J., Van Compernolle, B., Decyk, V., & Thorne, R. (2017). Electrostatic and whistler instabilities excited by an electron beam. *Physics of Plasmas*, *24*(7), 072116.

Birdsall, C. K., & Langdon, A. B. (2004). *Plasma physics via computer simulation.* CRC press.

Bohm, D., & Gross, E. P. (1949). Theory of plasma oscillations. b. excitation and damping of oscillations. *Physical Review*, *75*(12), 1864.

Brieda, L. (2019). *Plasma simulations by example.* CRC Press.

Chakrabarti, N., & Sengupta, S. (2009). Nonlinear interaction of electron plasma waves with electron acoustic waves in plasmas. *Physics of Plasmas*, *16*(7), 072311.

Changmai, S., & Bora, M. P. (2019). Photoemission driven electron two-stream instability (etsi) and evolution of plasma sheath. *Physics of Plasmas*, *26*(4), 042113.

Cowley, S. W. H. (2007). Magnetosphere of the earth. In D. Gubbins & E. Herrero-Bervera (Eds.), *Encyclopedia of geomagnetism and paleomagnetism* (pp. 656–664). Dordrecht: Springer Netherlands. Retrieved from https://doi.org/10.1007/978-1-4020-4423-6_205 doi: 10.1007/978-1-4020-4423-6_205

Crary, F., Goldman, M., Ergun, R., & Newman, D. (2001). Explanation for the simultaneous occurrence of bipolar structures and waves near ion-cyclotron harmonics in the auroral ionosphere. *Geophysical research letters*, *28*(15), 3059–3062.

Dalgarno, A., McElroy, M. B., & Moffett, R. (1963). Electron temperatures in the ionosphere. *Planetary and Space Science*, *11*(5), 463–484.

Dum, C. (1990). Simulation studies of plasma waves in the electron foreshock: The transition from reactive to kinetic instability. *Journal of Geophysical Research: Space Physics*, *95*(A6), 8111–8122.

Garrett, H. B., Kim, W., & Evans, R. W. (2016). Updating the jovian plasma and radiation environments: The latest results for 2015. *Journal of Spacecraft and Rockets*, *53*(4), 693–707.

Gary, S. P., & Tokar, R. L. (1985). The electron-acoustic mode. *The Physics of fluids*, *28*(8), 2439–2441.

Ginzburg, V., & Zhelezniakov, V. (1958). On the possible mechanisms of sporadic solar radio emission (radiation in an isotropic plasma). *Soviet Astronomy*, *2*, 653.

Goldman, M. V., Crary, F., Newman, D. L., & Oppenheim, M. (2000). Turbulence driven by two-stream instability in a magnetized plasma. *Physics of Plasmas*, *7*(5), 1732–1739.

Henri, P., Califano, F., Briand, C., & Mangeney, A. (2010). Vlasov-poisson simulations of electrostatic parametric instability for localized langmuir wave packets in the solar wind. *Journal of Geophysical Research: Space Physics*, *115*(A6).

Holman, G., & Benedict, S. (n.d.). *Solar Flare Theory table of contents.* `https://hesperia.gsfc.nasa.gov/sftheory/toc.htm`.

International Reference Ionosphere. (n.d.). `https://ccmc.gsfc.nasa.gov/modelweb/models/iri2016_vitmo.php`.

Jao, C.-S., & Hau, L.-N. (2016). Fluid theory and kinetic simulation of two-dimensional electrostatic streaming instabilities in electron-ion plasmas. *Physics of Plasmas*, *23*(11), 112110.

Karak, B. B., Mandal, S., & Banerjee, D. (2018). Double peaks of the solar cycle: an explanation from a dynamo model. *The Astrophysical Journal*, *866*(1), 17.

Kasaba, Y., Matsumoto, H., & Omura, Y. (2001). One-and two-dimensional simulations of electron beam instability: Generation of electrostatic and electromagnetic 2f p waves. *Journal of Geophysical Research: Space Physics*, *106*(A9), 18693–18711.

Khazanov, G. V., Chen, M. W., Lemon, C. L., & Sibeck, D. G. (2019). The magnetosphere-ionosphere electron precipitation dynamics and their geospace consequences during the 17 march 2013 storm. *Journal of Geophysical Research: Space Physics*, *124*(8), 6504–6523.

Koen, E. J., Collier, A. B., & Maharaj, S. K. (2012). Particle-in-cell simulations of beam-driven electrostatic waves in a plasma. *Physics of Plasmas*, *19*(4), 042101.

Langley, R. B. (2000). Gps, the ionosphere, and the solar maximum. *GPS world*, *11*(7), 44–49.

Lin, C., Burch, J., Shawhan, S., & Gurnett, D. (1984). Correlation of auroral hiss and upward electron beams near the polar cusp. *Journal of Geophysical*

Research: Space Physics, *89*(A2), 925–935.

Lu, Q., Wang, S., & Dou, X. (2005). Electrostatic waves in an electron-beam plasma system. *Physics of plasmas*, *12*(7), 072903.

Marif, H., & Lilensten, J. (2020). Suprathermal electron moments in the ionosphere. *Journal of Space Weather and Space Climate*, *10*, 22.

Miyake, T., Omura, Y., & Matsumoto, H. (2000). Electrostatic particle simulations of solitary waves in the auroral region. *Journal of Geophysical Research: Space Physics*, *105*(A10), 23239–23249.

Miyake, T., Omura, Y., Matsumoto, H., & Kojima, H. (1998). Two-dimensional computer simulations of electrostatic solitary waves observed by geotail spacecraft. *Journal of Geophysical Research: Space Physics*, *103*(A6), 11841–11850.

Muschietti, L., Roth, I., Ergun, R., & Carlson, C. (1999). Analysis and simulation of bgk electron holes. *Nonlinear Processes in Geophysics*, *6*(3/4), 211–219.

Newman, D., Goldman, M., Ergun, R., & Mangeney, A. (2001). Formation of double layers and electron holes in a current-driven space plasma. *Physical Review Letters*, *87*(25), 255001.

Omura, Y., Matsumoto, H., Miyake, T., & Kojima, H. (1996). Electron beam instabilities as generation mechanism of electrostatic solitary waves in the magnetotail. *Journal of Geophysical Research: Space Physics*, *101*(A2), 2685–2697.

Parks, G. K. (2019). *Physics of space plasmas: an introduction.* CRC Press.

Russell, C. T. (2010). *The mars plasma environment.* Springer Science & Business Media.

Sharifi, M. A., & Farzaneh, S. (2016). Local ionospheric modeling using the localized global ionospheric map and terrestrial gps. *Acta Geophysica*, *64*, 237–252.

Singh, N., Loo, S., Wells, B. E., & Deverapalli, C. (2000). Three-dimensional structure of electron holes driven by an electron beam. *Geophysical research letters*, *27*(16), 2469–2472.

Singh, S., Reddy, R., & Lakhina, G. (2009). Broadband electrostatic noise and low-frequency waves in the earth's magnetosphere. *Advances in space research*, *43*(12), 1940–1944.

Space Weather Prediction Center solar cycle progression. (n.d.). `https://www.swpc.noaa.gov/products/solar-cycle-progression`.

Tokar, R. L., & Gary, S. P. (1984). Electrostatic hiss and the beam driven electron acoustic instability in the dayside polar cusp. *Geophysical research letters*, *11*(12), 1180–1183.